Rotational motion of a magnetic vortex in a circular disk induced by injection of an electric current through an off-centered point contact

Hiroshi Tsukahara[1,2] and Hiroshi Imamura[1,*]

[1]*National Institute of Advanced Industrial Science and Technology (AIST), Spintronics Research Center, Tsukuba, Ibaraki 305-8568, Japan*

[2]*Institute of Materials Structure Science, High Energy Accelerator Research Organization (KEK), Tsukuba, Ibaraki 305-0801, Japan*

(Received 8 August 2014; revised manuscript received 10 December 2014; published 24 December 2014)

The dynamics of a magnetic vortex in a circular disk with an off-centered point contact is theoretically studied based on Thiele's equation and two-vortices model. It is shown that the steady-state rotational motion of a vortex core is induced by an electric current, and the threshold current of this rotational motion increases as the distance between the point contact and the center of the disk increases. The increase rate of the threshold current depends on the curling of the vortex because the Oersted field acts as an attractive or repulsive force between the vortex core and the point contact, depending on the curling of the vortex.

DOI: 10.1103/PhysRevB.90.214437 PACS number(s): 75.76.+j, 75.75.−c, 75.40.Gb, 75.70.Kw

I. INTRODUCTION

A magnetic vortex is a curling magnetic structure realized in submicrometer or micrometer-sized magnetic disks [1,2]. The magnetization curls in the disk plane to reduce the demagnetization energy except around the vortex center called "vortex core." In the vortex core, the magnetization has an out-of-plane component to reduce the exchange energy and at the center of the vortex core the magnetization points perpendicular to the disk plane. The magnetic configuration across the center of a vortex core is similar to that across the Bloch wall and the size of the vortex core is of the order of 10 nm. The dynamics of the magnetic vortex is well represented by the motion of the vortex core, which has been described theoretically by Thiele's equation [3].

In 1996 Slonczewski [4] and Berger [5] predicted that a spin-polarized electric current passing through a ferromagnet generates a torque on the magnetization in the ferromagnet. This torque, which is called spin-transfer torque (STT), can induce the steady-state rotational motion of a vortex core [6,7]. Compared with the uniform precession of magnetization in the nanopillar spin valve [8], the microwave voltage signal generated by the rotational motion of the vortex core has a very narrow line width, which has attracted much attention as a basic element of nanometer-sized microwave generators or sensors.

Most experiments of the current-induced dynamics of magnetic vortex have been done by using the spin-valve structure where the reference layer acted as a spin polarizer [9–17]. However, if the electrodes are attached so that the current is flowing in the in-plane direction, the dynamics of the vortex can be excited even without a spin-polarizer layer [18–20]. It is then natural to ask whether the dynamics of the vortex can be excited by injecting the current from the off-centered point contact to a magnetic disk, and if it can, how the dynamics of the vortex is affected by the curling of the vortex as well as the position of the point contact.

In this paper, we derive Thiele's equation for a magnetic vortex in a circular disk with an off-centered point contact. Solving the derived Thiele's equation, we show that the steady-state rotational motion of a vortex core appears as we expected. We also show that the threshold current of this rotational motion increases as the distance between the point contact and the center of the disk increases, and that it depends on the curling of the vortex.

II. MODEL AND METHOD

The system we consider is schematically shown in Fig. 1(a). A circular nano-pillar with radius R consists of top and bottom nonmagnetic electrodes, a magnetic layer having a magnetic vortex, and an insulating layer with a point contact. The origin of our coordinate system (x_1,x_2,x_3) is located at the center of the nanopillar on the bottom surface of the ferromagnetic layer. The thickness of the magnetic layer and the distance of the contact center from the origin are represented by L and X_c, respectively. The cross-section of the point contact is assumed to be circular. Figure 1(b) schematically shows the direction of the magnetization of a magnetic vortex in the magnetic layer. The directional cosine along the x_3 axis is represented by the blue scale.

In order to describe the dynamics of a magnetic vortex, we employ the two vortices model introduced by Guslienko *et al.* [21]. The direction of the magnetization $\boldsymbol{M}$ is indicated by the unit vector $\boldsymbol{m} = \boldsymbol{M}/M_s = (\sin\theta\cos\varphi, \sin\theta\sin\varphi, \cos\theta)$, where M_s is the saturation magnetization. In the two-vortices model, the azimuth angle φ is given by [22]

$$\varphi(\rho,\vartheta) = \mathrm{Arg}(\rho e^{i(\vartheta_c-\vartheta)} - \rho_c) + \mathrm{Arg}\left(\rho e^{i(\vartheta_c-\vartheta)} - \frac{R^2}{\rho_c}\right) + \varrho\frac{\pi}{2} + \vartheta_c, \quad (1)$$

(ρ_c,ϑ_c) denotes the position of the vortex core, (ρ,ϑ) are the polar coordinates in the x_1x_2 plane and ϱ represents the curling. When $\varrho = 1$ (-1), the vortex has clockwise (counter clockwise) curling in x_1x_2 plane. The polar coordinate is assumed to take the bell shape as [23]

$$\theta = \begin{cases} \pi/2 & |\boldsymbol{x}-\boldsymbol{X}| > b \\ \cos^{-1}\left(p\frac{b^2-|\boldsymbol{x}-\boldsymbol{X}|^2}{b^2+|\boldsymbol{x}-\boldsymbol{X}|^2}\right) & |\boldsymbol{x}-\boldsymbol{X}| < b \end{cases}, \quad (2)$$

*h-imamura@aist.go.jp

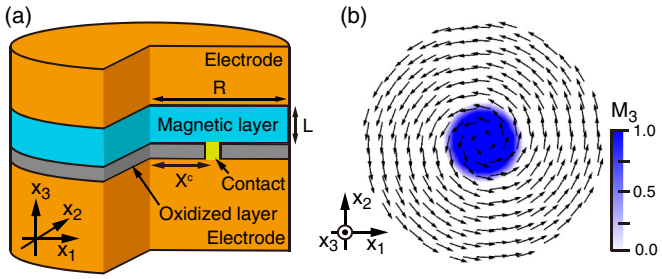

FIG. 1. (Color online) Schematic illustration of (a) the nanopillar with single nano point contact and (b) the magnetic vortex in the magnetic layer. The magnetic layer thickness is L and the radius of the pillar is R. The distance between the origin of our coordinates and the contact center is $\boldsymbol{X}^{\mathrm{c}}$. The directional cosine of the magnetization along x_3 axis is represented by the blue scale.

where b represents the radius of the magnetic vortex and $\boldsymbol{X}$ is the position of the vortex core and $p = \pm 1$ which represents the polarity of the magnetic vortex in this model.

According to Ohm's law the electric current flowing in the nanopillar is expressed as $\boldsymbol{j} = \sigma \nabla \Phi(\boldsymbol{x})$ where $\boldsymbol{j}$ denotes the electric current density, $\Phi(\boldsymbol{x})$ is the electric potential and σ is the conductivity. Assuming that the size of the point contact is much smaller than the radius of the nanopillar, the electric potential can be expressed as [24]

$$\Phi(r,x_3) = \frac{V}{2}\left[1 - \frac{\pi}{2}\tan^{-1}\left(\frac{1}{\eta}\right)\right], \tag{3}$$

where V is a voltage applied to the electrodes and $r = \sqrt{x_1^2 + x_2^2}$. Here, η is a component of an oblate spheroidal coordinate (η,ζ,ϕ) that is related to the Cartesian coordinates as

$$x_1 = a\sqrt{(1+\eta^2)(1-\zeta^2)}\cos\phi, \tag{4}$$

$$x_2 = a\sqrt{(1+\eta^2)(1-\zeta^2)}\sin\phi, \tag{5}$$

$$x_3 = a\eta\zeta, \tag{6}$$

where a represents the radius of the point contact. Each component of the current density is obtained as

$$j_1 = \frac{\mathcal{J}}{4S_c}\frac{\sqrt{(1+\eta^2)(1-\zeta^2)}}{(\eta^2+\zeta^2)(\eta^2+1)}\cos\phi, \tag{7}$$

$$j_2 = \frac{\mathcal{J}}{4S_c}\frac{\sqrt{(1+\eta^2)(1-\zeta^2)}}{(\eta^2+\zeta^2)(\eta^2+1)}\sin\phi, \tag{8}$$

$$j_3 = \frac{\mathcal{J}}{4S_c}\frac{\zeta}{\eta^2+\zeta^2}, \tag{9}$$

where $\mathcal{J} = 2\pi a\sigma V$ is the total current and S_c is the cross-section area of the point contact. The Oersted field $\boldsymbol{H}^{\mathrm{Oe}}$ generated by $\boldsymbol{j}$ can be calculated using the Biot-Savart law [25].

The equation of motion of the magnetization $\boldsymbol{M}$ is given by the Landau-Lifshitz-Gilbert equation with Zhang-Li's spin transfer torque [26],

$$\frac{d\boldsymbol{M}}{dt} = -|\gamma|(\boldsymbol{M}\times\boldsymbol{H}_{\mathrm{eff}}) + \frac{\alpha}{M_s}\boldsymbol{M}\times\frac{d\boldsymbol{M}}{dt} - \frac{b_J}{M_s^2}\boldsymbol{M}\times(\boldsymbol{M}\times(\boldsymbol{j}\cdot\nabla)\boldsymbol{M}) - \xi\frac{b_J}{M_s}\boldsymbol{M}\times(\boldsymbol{j}\cdot\nabla)\boldsymbol{M}, \tag{10}$$

where t is time, $\boldsymbol{H}_{\mathrm{eff}}$ is the effective magnetic field, γ is the gyromagnetic ratio, and α is the Gilbert damping constant [20]. The coupling constant between the current and the magnetization is given by $b_J = (P\mu_B)/[eM_s(1+\xi^2)]$, where P is the spin polarization of the current, μ_B is the Bohr magneton, e is the elementary charge, and $\xi = \tau_{\mathrm{ex}}/\tau_{\mathrm{sf}}$ is the degree of nonadiabaticity, which is the ratio between the exchange relaxation time τ_{ex} and the spin-flip relaxation time τ_{sf}. Following Ref. [27], we rewrite Eq. (10) in the following simple form:

$$|\gamma|\boldsymbol{M}\times(\boldsymbol{H}_{\mathrm{eff}} + \boldsymbol{H}^g + \boldsymbol{H}^\alpha + \boldsymbol{H}^{S_1} + \boldsymbol{H}^{S_2}) = 0, \tag{11}$$

where $\boldsymbol{H}_{\mathrm{eff}}$ is the effective magnetic field, which originally appeared in the LLG equation, and the other effective magnetic fields are defined as

$$\boldsymbol{H}^g = -\frac{1}{|\gamma|M_s}\boldsymbol{M}\times\frac{d\boldsymbol{M}}{dt}, \tag{12}$$

$$\boldsymbol{H}^\alpha = -\frac{\alpha}{M_s}\frac{d\boldsymbol{M}}{dt}, \tag{13}$$

$$\boldsymbol{H}^{S_1} = \frac{b_J}{|\gamma|M_s^2}\boldsymbol{M}\times(\boldsymbol{j}\cdot\nabla)\boldsymbol{M}, \tag{14}$$

$$\boldsymbol{H}^{S_2} = \frac{\xi b_J}{|\gamma|M_s}(\boldsymbol{j}\cdot\nabla)\boldsymbol{M}. \tag{15}$$

Assuming that the magnetization is a function of $\boldsymbol{X}-\boldsymbol{x}$, each component of the force density f_i due to the field $\boldsymbol{H}$ is given by

$$f_i = \boldsymbol{H}\cdot\frac{\partial\boldsymbol{M}}{\partial X_i} = -\boldsymbol{H}\cdot\frac{\partial\boldsymbol{M}}{\partial x_i}. \tag{16}$$

The force densities due to the fields $\boldsymbol{H}^g$ and $\boldsymbol{H}^\alpha$ are, respectively, given by

$$f_i^g = -\varepsilon_{ijk}v_j g_k, \quad f_i^\alpha = d_{ij}v_j, \tag{17}$$

where ε_{ijk} is the Levi-Civita antisymmetric tensor, $v_i = dX_i/dt$ and

$$g_k = -\frac{1}{2|\gamma|M_s^2}\varepsilon_{\mu\nu k}\varepsilon_{lmn}M_l\frac{\partial M_m}{\partial x_\mu}\frac{\partial M_n}{\partial x_\nu}, \tag{18}$$

$$d_{ij} = -\frac{\alpha}{|\gamma|M_s}\frac{\partial M_n}{\partial x_j}\frac{\partial M_n}{\partial x_i}. \tag{19}$$

Here the Einstein convention of summation is assumed. In the same manner, $f_i^{S_1}$ and $f_i^{S_2}$ are obtained as

$$f_i^{S_1} = \frac{b_J}{|\gamma|M_s^2}\varepsilon_{lnm}M_l\frac{\partial M_m}{\partial x_i}\frac{\partial M_n}{\partial x_\mu}j_\mu, \tag{20}$$

$$f_i^{S_2} = -\frac{\xi b_J}{|\gamma|M_s}\frac{\partial M_n}{\partial x_i}\frac{\partial M_n}{\partial x_\mu}j_\mu. \tag{21}$$

Integrating the force densities of Eq. (17) over the magnetic layer, we obtain the forces due to $\boldsymbol{H}^g$ and $\boldsymbol{H}^\alpha$ as

$$\boldsymbol{F}^g = \boldsymbol{G} \times \boldsymbol{v}, \quad \boldsymbol{F}^\alpha = D\boldsymbol{v}, \tag{22}$$

where $G_i = 2\pi L q p \delta_{i3}/\gamma$ with topological charge q and $D = D_{ii}$ with $D_{ij} = \int d\boldsymbol{x} d_{ij}$. The forces due to $\boldsymbol{H}^{S_1}$ and $\boldsymbol{H}^{S_2}$ are also obtained as

$$F_i^{S_1} = \varepsilon_{ij3} \int d\boldsymbol{r} \frac{b_J}{2|\gamma| M_s^2} \varepsilon_{\mu\nu 3} \left(\frac{\partial \boldsymbol{M}}{\partial x_\mu} \times \frac{\partial \boldsymbol{M}}{\partial x_\nu} \right) \cdot \boldsymbol{M} J_j, \tag{23}$$

$$F_i^{S_2} = -\frac{\xi b_J}{|\gamma| M_s} \int d\boldsymbol{r} \frac{\partial M_n}{\partial x_i} \frac{\partial M_n}{\partial x_\mu} J_\mu, \tag{24}$$

where $J_i = \int dx_3 j_i$ and $\boldsymbol{r} = (x_1, x_2)$.

The remaining forces due to the effective field $\boldsymbol{H}_{\rm eff}$ are obtained as follows. Introducing the potential energy of the effective field W, the force can be expressed as $F_i = -\partial W/\partial X_i$. Since the magnetic vortex moves in the magnetic disk with finite radius, W consists of the potential energy caused by a vortex shift and Oersted field. Therefore it is convenient to separate W into two terms: one is W^s arising from the shift of the vortex core from the center of the disk, and the other is $W^{\rm Oe}$ arising from the Oersted field. According to Refs. [28,29], the force $\boldsymbol{F}^s$ is proportional to the position of the vortex core, X, as $\boldsymbol{F}^s = -k^{\rm ms}\boldsymbol{X}$, and the proportional coefficient is given by

$$k^{\rm ms} = \frac{4M_s^2 L^2}{3R} \frac{2\mathcal{R} - 1}{1 - (s/2)^2} \tag{25}$$

with $s = |\boldsymbol{X}|/R$ and $\mathcal{R} \sim 0.916$. The force $F^{\rm Oe}$ is obtained by numerically calculating $W^{\rm Oe} = -\int d\boldsymbol{x} \boldsymbol{H}^{\rm Oe} \cdot \boldsymbol{M}$ and $F_i^{\rm Oe} = -\partial W^{\rm Oe}/\partial X_i$.

Finally, the equation of motion for analysis of the dynamics of a magnetic vortex in a circular disk induced by the injection of an electric current through an off-centered point contact is obtained as

$$\boldsymbol{G} \times \boldsymbol{v} + D\boldsymbol{v} - k^{\rm ms}\boldsymbol{X} + \boldsymbol{F}^{\rm Oe} + \boldsymbol{F}^{S_1} + \boldsymbol{F}^{S_2} = 0, \tag{26}$$

which is the direct extension of Thiele's equation for uniform electric current distribution [30,31]. Note that the forces from the electric current are functions of $\boldsymbol{X}^{\rm c}$. Equation (26) is numerically solved by using the fourth-order Runge-Kutta method. The following material parameters are assumed in our calculation: $\alpha = 0.01$, $M_{\rm s} = 6.5 \times 10^5$ A/m, $L = 15$ nm, $R = 100.0$ nm, $a = 2.0$ nm, $b = 5$ nm, $P = 1.0$, $\xi = 0.05$, and $p = 1.0$.

III. RESULTS AND DISCUSSION

Before showing the results of the dynamics let us look at the direction and magnitude of the forces arising from the applied electric current, $\boldsymbol{F}^{S_1}$, $\boldsymbol{F}^{S_2}$, and $\boldsymbol{F}^{\rm Oe}$. In Figs. 2(a) and 2(b), we plot the $x_1(x_2)$-component of the each force against the position of the point contact by the solid (dotted) lines. The vortex core is located at the center of the disk, i.e., $|\boldsymbol{X}| = 0$, and the point contact is located at $\boldsymbol{X}^{\rm c} = (X_1^{\rm c}, 0)$. The curling of the vortex is counter-clockwise (CCW) in Fig. 2(a), while it is clockwise (CW) in Fig. 2(b). Since the point contact is on the x_1 axis the $x_1(x_2)$ component of the force represents the restoring(rotational) force. At $X_1^{\rm c} = 0$, all forces are zero and

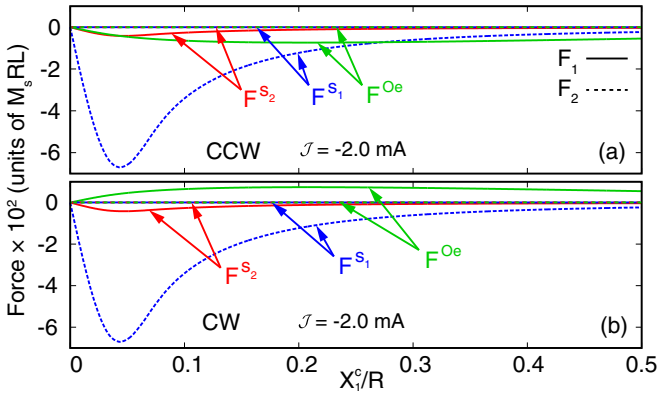

FIG. 2. (Color online) The forces induced by the electric current are plotted as a function of $X_1^{\rm c}$ for a magnetic vortex with (a) counterclockwise and (b) clockwise curling. The blue, red, and green lines represent $\boldsymbol{F}^{S_1}$, $\boldsymbol{F}^{S_2}$, and $\boldsymbol{F}^{\rm Oe}$, respectively. The solid (dotted) lies denote the forces in the x_1 (x_2) direction.

the vortex core does not move because of the axial symmetry around the x_3 axis. Even for the finite value of $X_1^{\rm c}$, the rotational component of $\boldsymbol{F}^{S_2}$ and $\boldsymbol{F}^{\rm Oe}$, and the restoring component of $\boldsymbol{F}^{S_1}$ vanish because the system has reflectional symmetry about the x_1 axis. With increasing $X_1^{\rm c}$, the magnitudes of $\boldsymbol{F}^{S_1}$ and $\boldsymbol{F}^{S_2}$ decrease rapidly while the magnitude of $\boldsymbol{F}^{\rm Oe}$ decreases slowly. It should be noted that the force $\boldsymbol{F}^{\rm Oe}$ changes its sign depending on the curling as shown in Figs. 2(a) and 2(b). For the vortex with CCW (CW) curling, $\boldsymbol{F}^{\rm Oe}$ acts as an repulsive (attractive) force between the vortex core and the point contact.

Let us move on to the rotational motion of the vortex core induced by the electric current. Figure 3 shows trajectories of the vortex core with (a) CCW curling, (b) CCW curling under no Oersted field, and (c) CW curling. Hereafter the abbreviation "NOF" stands for the magnetic vortex having CCW curling under no Oersted field. In these calculations, the point contact is located at $X_1^{\rm c} = 0.4$ nm and the amplitude of the electric current is set at $\mathcal{J} = -2.0$ mA. Once the electric current is applied the vortex core starts to rotate from the equilibrium position due to $\boldsymbol{F}^{S_1}$ and, finally, it rotates on a circular trajectory. The time evolution of X_1 is also shown in Fig. 3(d). The oscillation amplitude saturates after about ten nanoseconds, and the oscillation amplitudes and frequencies depend on the magnetic vortex curling and the Oersted field. As mentioned before, $\boldsymbol{F}^{\rm Oe}$ is an attractive (repulsive) force between the point contact and the vortex core with CW (CCW) curling, and the radius of the steady-state trajectory of the CW curling is smaller than that of the CCW curling. The radius of the steady-state trajectory of NOF is intermediate between those of CW and CCW because $\boldsymbol{F}^{\rm Oe} = 0$. The oscillation frequency is the smallest (largest) for CCW (CW) curling as shown in Fig. 3(d).

Next we show how the magnetic vortex oscillation is modified by changing the position of the point contact, $X_1^{\rm c}$. The steady-state trajectories for $X_1^{\rm c} = 0.4$ and 10.0 nm are shown in Figs. 4(a) and 4(b), respectively. The amplitude of the electric current is set at $\mathcal{J} = -2.0$ mA. The trajectories for CCW, NOF, and CW are represented by the red, green, and blue curves, respectively. As shown in these figures, the steady-state trajectories are almost circular, and their centers are indicated

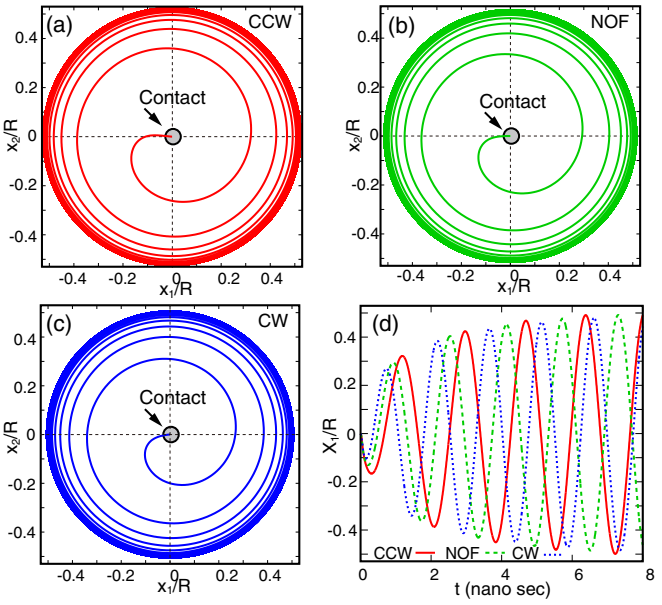

FIG. 3. (Color online) The trajectories of the magnetic vortex core with (a) CCW curling, (b) CCW curling under no Oersted field applied, and (c) CW curling. The gray circles indicate the point contact. (d) The x_1 component of the vortex core, X_1, for CCW, NOF, and CW is plotted as a function of t by the red-solid, green-dashed, and blue-dotted lines, respectively. For all results, the amplitude of the electric current is fixed at $\mathcal{J} = -2.0$ mA.

by dots of the same color. For $X_1^c = 0.4$ nm, it is hard to distinguish the position of the trajectory centers. However, for $X_1^c = 10.0$ nm, the trajectory center of CW curling moves to the contact center, while that of CCW curling moves in the opposite direction. If the Oersted field is neglected, the trajectory center hardly moves from the origin.

The current dependence of the oscillation amplitudes and frequencies for CCW, NOF and CW are shown in Figs. 5(a)–5(f). One can see that the current dependencies of the amplitudes are almost the same for CCW, NOF, and CW, while those of the frequencies strongly depend on the magnetic vortex curling and Oersted field [32–34]. Because $\boldsymbol{F}^{\mathrm{Oe}}$ is an attractive force in the case of the CW curling, the frequency is enhanced as the intensity of electric current

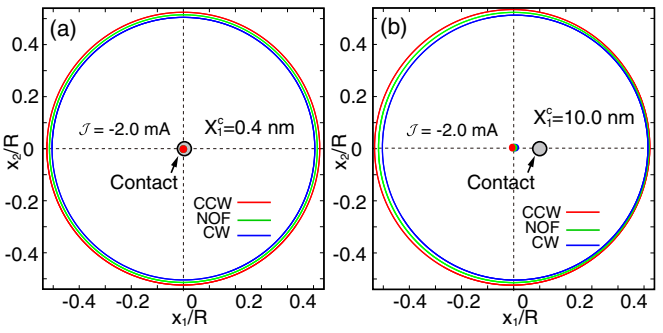

FIG. 4. (Color online) The steady-state trajectories of the vortex core for CCW, NOF and CW. The amplitude of the electric current is $\mathcal{J} = -2.0$ mA, and the point contact is located at (a) $X_1^c = 0.4$ and (b) 10.0 nm. The solid circles denote the position of the point contact.

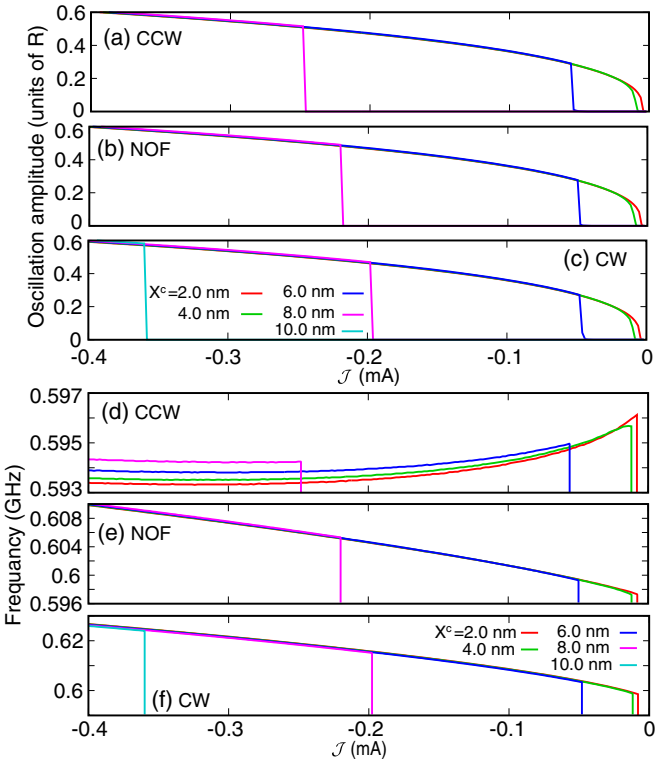

FIG. 5. (Color online) The oscillation amplitudes for CCW, NOF, and CW are plotted as a function of $\mathcal{J}$ in (a), (b), and (c), respectively. The oscillation frequencies for CCW, NOF, and CW are plotted as a function of $\mathcal{J}$ in the panels (d), (e), and (f), respectively. For all panels, the position of the point contact, X_1^c varies from 2.0 to 10.0 nm.

increases. Even if we neglect the Oersted field, the frequency slightly increases due to the nonlinear effects of the vortex shift. By stark contrast, the frequency of the CCW curling decreases as the intensity of electric current increases because $\boldsymbol{F}^{\mathrm{Oe}}$ weakens the restoring force. However, the shapes of the frequency curve as a function of $\mathcal{J}$ are almost unchanged for all values of $\boldsymbol{X}^c$. The jump in Figs. 5(a)–5(f) indicates the value of the threshold current for the rotation of the vortex core, which depends on the vortex curling, Oersted field, and X_1^c.

In Fig. 6, the threshold currents for CCW, NOF, and CW are plotted as functions of X_1^c. For $X_1^c < 5$ nm, the threshold

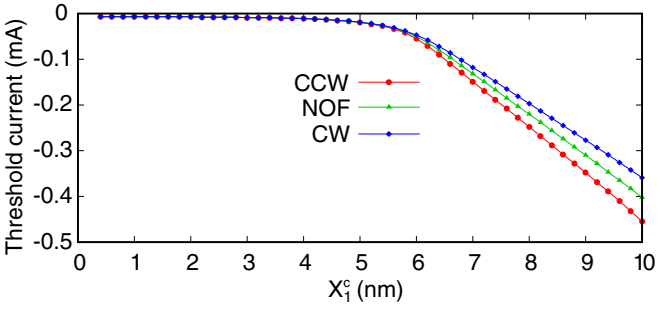

FIG. 6. (Color online) The threshold currents for CCW, NOF, and CW are plotted as a function of X_1^c by the red, green, and blue lines, respectively.

currents are almost zero for all cases. The differences among the threshold currents of CCW, NOF, and CW increase rapidly for $X_1^c > 5$ nm. The absolute value of the threshold current for the magnetic vortex with CCW curling is larger than that for the magnetic vortex with CW curling because the restoring force is weakened (enhanced) by $\boldsymbol{F}^{\mathrm{Oe}}$ between the center of the disk and the point contact for CW (CCW) curling.

IV. SUMMARY

We derived Thiele's equation for the magnetic vortex in the circular disk with an off-centered point contact and performed calculations of the vortex core dynamics by solving the derived equation. All forces arising from the applied electric current are zero when the point contact is located at the center of the circular disk. Even if the point contact is off-centered, the rotational component of $\boldsymbol{F}^{S_2}$ and $\boldsymbol{F}^{\mathrm{Oe}}$, and the restoring component of $\boldsymbol{F}^{S_1}$ vanish due to the reflectional symmetry of the system. Once the electric current is applied, the vortex core starts to rotate from the equilibrium position due to $\boldsymbol{F}^{S_1}$ and the trajectories of the steady rotation are circular, independently of the vortex curling and the Oersted field. The oscillation amplitude of the vortex having CW (CCW) curling is the smallest (largest) and the frequency of the vortex with CW (CCW) curling is the largest (smallest) because the restoring force is enhanced (weakened) due to $\boldsymbol{F}^{\mathrm{Oe}}$. Although the oscillation amplitude and frequency hardly depend on the position of the point contact, the threshold current depends on it. The absolute value of threshold current for the rotational motion increases as the distance between the point contact and the center of the disk increases. In the case of CCW (CW) curling, the rate of increase is the largest (smallest) because the restoring force is enhanced (weakened) by $\boldsymbol{F}^{\mathrm{Oe}}$ between the center of the circular disk and the vortex core.

ACKNOWLEDGMENTS

We would like to thank T. Taniguchi, H. Arai, K. Miyake, and M. Sahashi for valuable discussions. This work was partially supported by JSPS KAKENHI Grant No. 23226001.

[1] T. Shinjo, T. Okuno, R. Hassdorf, K. Shigeto, and T. Ono, Science **289**, 930 (2000).
[2] A. Wachowiak, J. Wiebe, M. Bode, O. Pietzsch, M. Morgenstern, and R. Wiesendanger, Science **298**, 577 (2002).
[3] A. A. Thiele, Phys. Rev. Lett. **30**, 230 (1973).
[4] J. C. Slonczewski, J. Magn. Magn. Mater. **159**, L1 (1996).
[5] L. Berger, Phys. Rev. B **54**, 9353 (1996).
[6] A. Dussaux, B. Georges, J. Grollier, V. Cros, A. V. Khvalkovskiy, A. Fukushima, M. Konoto, H. Kubota, K. Yakushiji, S. Yuasa, K. A. Zvezdin, K. Ando, and A. Fert, Nat. Commun. **1**, 8 (2010).
[7] K. Y. Guslienko, G. R. Aranda, and J. Gonzalez, J. Phys.: Conf. Ser. **292**, 012006 (2011).
[8] S. I. Kiselev, J. C. Sankey, I. N. Krivorotov, N. C. Emley, R. J. Schoelkopf, R. A. Buhrman, and D. C. Ralph, Nature (London) **425**, 380 (2003).
[9] O. Ozatay, N. C. Emley, P. M. Braganca, A. G. Garcia, G. D. Fuchs, I. N. Krivorotov, R. A. Buhrman, and D. C. Ralph, Appl. Phys. Lett. **88**, 202502 (2006).
[10] D. V. Berkov and N. L. Gorn, J. Appl. Phys. **99**, 08Q701 (2006).
[11] M. R. Pufall, W. H. Rippard, M. L. Schneider, and S. E. Russek, Phys. Rev. B **75**, 140404(R) (2007).
[12] G. Consolo, L. Lopez-Diaz, L. Torres, G. Finocchio, A. Romeo, and B. Azzerboni, Appl. Phys. Lett. **91**, 162506 (2007).
[13] Q. Mistral, M. van Kampen, G. Hrkac, Joo-Von Kim, T. Devolder, P. Crozat, C. Chappert, L. Lagae, and T. Schrefl, Phys. Rev. Lett. **100**, 257201 (2008).
[14] M. A. Hoefer, T. J. Silva, and Mark W. Keller, Phys. Rev. B **82**, 054432 (2010).
[15] R. M. Otxoa, M. Manfrini, T. Devolder, J.-V. Kim, W. van Roy, L. Lagae, and C. Chappert, Phys. Status Solidi B **248**, 1615 (2011).
[16] M. Takagishi, H. N. Fuke, S. Hashimoto, H. Iwasaki, S. Kawasaki, R. Shiozaki, and M. Sahashi, J. Appl. Phys. **105**, 07B725 (2009).
[17] K. Miyake, Y. Okutomi, H. Tsukahara, H. Imamura, and M. Sahashi, Appl. Phys. Express **6**, 113001 (2013).
[18] J. Shibata, Y. Nakatani, G. Tatara, H. Kohno, and Y. Otani, Phys. Rev. B **73**, 020403 (2006).
[19] S. Kasai, Y. Nakatani, K. Kobayashi, H. Kohno, and T. Ono, Phys. Rev. Lett. **97**, 107204 (2006).
[20] M. Najafi, B. Krüger, S. Bohlens, M. Franchin, H. Fangohr, A. Vanhaverbeke, R. Allenspach, M. Bolte, U. Merkt, D. Pfannnkuche, D. P. F. Möller, and G. Meier, J. Appl. Phys. **105**, 113914 (2009).
[21] K. Yu. Guslienko, J. Nanosci. Nanotechnol. **8**, 2745 (2008).
[22] A. Dussaux, A. V. Khvalkovskiy, P. Bortolotti, J. Grollier, V. Cros, and A. Fert, Phys. Rev. B **86**, 014402 (2012).
[23] N. A. Usov and S. E. Peschany, J. Magn. Magn. Mater. **118**, L290 (1993).
[24] A. G. M. Jansen, A. P. Van Gelder, and P. Wyder, J. Phys. C **13**, 6073 (1980).
[25] J. D. Jackson, *Classical Electrodynamics*, 3rd ed. (Wiley, New York, 1998), p. 175.
[26] S. Zhang and Z. Li, Phys. Rev. Lett. **93**, 127204 (2004).
[27] J. Kim and S.-B. Choe, J. Magn. **12**, 113 (2007).
[28] K. Yu. Guslienko, X. F. Han, D. J. Keavney, R. Divan, and S. D. Bader, Phys. Rev. Lett. **96**, 067205 (2006).
[29] Y. Gaididei, V. P. Kravchuk, and D. D. Sheka, Int. J. Quantum Chem. **110**, 83 (2010).
[30] A. Thiaville, Y. Nakatani, J. Miltat, and Y. Suzuki, Europhys. Lett. **69**, 990 (2005).
[31] B. Krüger, A. Drews, M. Bolte, U. Merkt, D. Pfannkuche, and G. Meier, Phys. Rev. B **76**, 224426 (2007).
[32] Y.-S. Choi, K.-S. Lee, and S.-K. Kim, Phys. Rev. B **79**, 184424 (2009).
[33] A. V. Khvalkovskiy, J. Grollier, A. Dussaux, Konstantin A. Zvezdin, and V. Cros, Phys. Rev. B **80**, 140401(R) (2009).
[34] A. V. Khvalkovskiy, J. Grollier, N. Locatelli, Ya. V. Gorbunov, K. A. Zvezdin, and V. Cros, Appl. Phys. Lett. **96**, 212507 (2010).